OPTIMAL DESIGN OF AXIAL NOBLE METAL DISTRIBUTION FOR IMPROVING THE PERFORMANCE OF A DUAL MONOLITHIC CATALYTIC CONVERTER

Kim Y.-D., Shim S.-M., Jeong S.-J., and Kim W.-S.*
*Author for correspondence
Department of Mechanical Engineering,
Hanyang University, 1271 Sa 3-dong,
Ansan, Gyeonggi-do 426-791,
South Korea,
E-mail: wskim@hanyang.ac.kr

ABSTRACT

In practical applications, monolithic catalytic converters are operated at non-isothermal conditions. In this case, the active metal distribution along the length of the converter may influence its performance. Indeed, better conversions can be achieved by controlling the distribution of the same quantity of active material. In this study, we used a one-dimensional catalyst model to predict the transient thermal and conversion characteristics of a dual monolithic catalytic converter with Platinum/Rhodium (Pt/Rh) catalysts. The optimal design of a longitudinal noble metal distribution of a fixed amount of catalyst is investigated to obtain the best performance of a dual monolithic catalytic converter by using a micro genetic algorithm with consideration of heat transfer, mass transfer, and chemical reaction in the monolith during FTP-75 cycle. The optimal design for the optimal axial distribution of the catalyst is determined by solving the multi-objective optimization problems which are to minimize both the CO cumulative emissions during FTP-75 cycle, and the difference between the integral value of a catalyst distribution function over the monolith volume and catalytic surface area per unit monolith volume.

INTRODUCTION

Nowadays, controlling emissions is not simply a case of engine design and engine management. Exhaust gas after-treatment systems play an important role, as current and future automobile emission regulations become more stringent. The achievement of tighter emission standards for gasoline vehicles is based on reduction of cold-start emissions by attaining faster light-off of the catalytic converter. Because automotive catalysts operate inefficiently until they reach their light-off temperature at typically 600K or higher, about 60-80% of total HC emissions over the NEDC and the FTP-75 cycle are emitted within the first 200 sec of the cold start phase. Therefore, many

NOMENCLATURE

A	[m²]	Open frontal area of the monolith
$a(x)$	[m²/m³]	Catalyst distribution function
a_0	[m²/m³]	Catalytic surface area per unit monolith volume
c_i	[mole fraction]	Concentration of species i
c_p	[J/kgK]	Specific heat capacity
D_i	[m²/s]	Binary diffusion coefficient of species i in the mixture
$E_{a,k}$	[J/kmol]	Activation energy of reaction k
$F(X)$	[-]	Objective function
G	[-]	Inhibition factor
GSA	[m²/ m³]	Geometrical surface area per unit reactor volume
h_t	[W/m²K]	Heat transfer coefficient
$\Delta H_{a,j}$	[J/kmol]	Adsorption heat
ΔH_k	[J/kmol]	Enthalpy of reaction k
$k_{a,j}$	[-]	Pre-exponential factor of adsorption equilibrium constant
$k_{m,i}$	[m/s]	Mass transfer coefficient of species i in the mixture
$k_{0,k}$	[molK/m²s]	Pre-exponential factor of rate constant k
K_j	[-]	Adsorption equilibrium constant
K_p	[-]	Chemical equilibrium constant
L	[m]	Channel length
m	[kg/s]	Mass flow rate
M_i	[kg/kmol]	Molecular weight of species i
N_R	[-]	Number of reactions
r_k	[mol/m²s]	Rate of reaction k
R_g	[J/molK]	Universal gas constant
t	[s]	Time
T	[K]	Temperature
v_{ik}	[-]	Stoichiometric coefficient of species i in the reaction k
V_m	[m³]	Monolith volume
w_i	[mass fraction]	Concentration of species i
x	[m]	Axial coordinate
X	[-]	Vector of the design variables

Greek symbols

α	[-]	Coefficient included in the catalyst distribution function
β	[-]	Coefficient included in the catalyst distribution function
ε	[-]	Void fraction of the monolith
λ	[W/mK]	Thermal conductivity
ρ	[kg/m³]	Density

Subscripts and superscripts

g	gas
i	Species index
in	Inlet (superscript)
k	Reaction index
L	Channel length
s	Solid
x	Axial coordinate

attempts have been performed to reduce the time needed for catalysts to reach their light-off temperature.

To improve the light-off performance and conversion efficiency of catalytic converters, parametric investigations on the effect of various design factors (cell density, wall thickness, length and diameter of the monolith, channel geometry, and composition of catalyst and washcoat, axial catalyst distribution etc.) on the performance of the monolith have been performed in a number of numerical and experimental studies. In particular, the effect of non-uniform axial distribution with a simple chemical reaction and operating conditions on the performance of the catalytic converter has been examined [1-8]. Oh and Cavendish [1] examined the light-off behavior of three Pt distribution profiles along the reactor length, and showed that the light-off performance is improved substantially when the noble metal is concentrated in the upstream section of the monolith. It is also well known that non-uniform catalyst distribution within a pellet can provide better performance as compared to uniform catalysts [2]. Psyllos and Philippopoulos [3] showed that the performance of catalysts with parabolic axial catalyst distribution for CO oxidation is better than monoliths with uniform axial catalyst distribution. It was shown for the reaction of methane oxidation that non-uniform catalyst distributions have the potential to achieve lower thermal stresses [4]. Melis *et al.* [5] examined the effect of axial distribution of a fixed amount of catalyst on the performance of an isothermal reactor, in which both heterogeneous and homogeneous reactions occur. They showed that the optimal distribution depends on strongly whether or not interactions exist between the heterogeneous and homogeneous reactions.

The aforementioned studies indicated that non-uniform catalyst distribution can improve the performance of the catalytic converter. However, an optimal catalyst distribution was not identified. Khanaev *et al.* [6] showed that in the adiabatic reactor the optimal profile is the one that monotonically decreases along the bed length in the case of an exothermal reaction and monotonically increases in the case of an endothermal reaction, while the uniform active component distribution profile is optimal for a first-order reaction in an isothermal reactor. The optimization of the loading pattern for improving warm-up catalyst performance with an optimization algorithm has been performed by Tronci *et al.* [7] and Kim and Kim [8]. They showed that the high noble metal surface area in the upstream section of the monolith significantly minimizes the cold start pollutant emissions.

In the present work, while keeping the catalytic surface area per unit monolith volume constant, the optimal design of a longitudinal noble metal distribution to obtain the best performance of a dual monolithic catalytic converter is performed by using a micro genetic algorithm with consideration of heat transfer, mass transfer, and chemical reaction in the monolith during FTP-75 cycle. Prior to the optimization of the dual-catalyst converter, the pre-exponential factor and activation energy of each reaction for catalyst are modified to achieve the reasonable agreement with experimental data under typical FTP-75 cycle of automobile application. The optimal design for the optimal axial distribution of the catalyst is determined by solving the multi-objective optimization problems to minimize both the CO cumulative emissions during FTP-75 cycle, and the difference between the integral value of a catalyst distribution function over the monolith volume and catalytic surface area per unit monolith volume.

MODEL DESCRIPTION

Catalyst Model

The structure of monolithic catalytic converters used in automotive exhaust after-treatment systems consists of a number of small parallel channels, inducing a laminar flow field inside. The catalytic material is impregnated on a porous high surface area material, called a washcoat, which covers the channels of the substrate along their wetted perimeter. The diffusion of reactants through the gas phase and the porous washcoat is followed by catalytic reactions, occurring on precious metal surface sites at the gas-solid interface inside the porous washcoat. The physical and chemical processes in a monolithic reactor are depicted in Figure 1.

The transient one-dimensional equations for the gas phase heat and mass transfer are:

$$\varepsilon \cdot \rho_g \cdot c_{p,g} \cdot \frac{\partial T_g}{\partial t} = $$
$$-\frac{m}{A} \cdot c_{p,g} \cdot \frac{\partial T_g}{\partial x} + \varepsilon \cdot \lambda_g \cdot \frac{\partial^2 T_g}{\partial x^2} + h_t(x) \cdot GSA \cdot (T_s - T_g) \quad (1)$$

$$\varepsilon \cdot \rho_g \cdot \frac{\partial w_{i,g}}{\partial t} = $$
$$-\frac{m}{A} \cdot \frac{\partial w_{i,g}}{\partial x} + \varepsilon \cdot D_i \cdot \rho_g \cdot \frac{\partial^2 w_{i,g}}{\partial x^2} - \rho_g \cdot k_{m,i}(x) \cdot GSA \cdot (w_{i,g} - w_{i,s}) \quad (2)$$

where D_i denotes the binary diffusion coefficient of species i in the mixture j [9] and the heat transfer coefficient h_t and the mass transfer coefficient k_m in equations (1) and (2) are dependent on the length of the substrate [10].
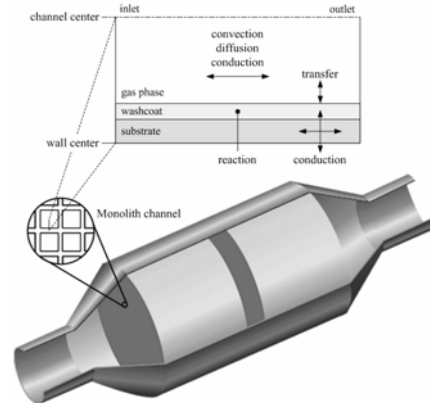

Figure 1 Relevant physical and chemical phenomena in the gas phase, washcoat, and substrate.

Table 1 Input data for dual-catalyst simulation.

Input data		
Precious metal ratio	5/1	Pt/Rh
Precious metal loading	26.9	g/ft^3
Substrate frontal area	99.87	m^2
Substrate cell density	400	cpsi
Substrate length	0.0903	m
Substrate thickness	1.65×10^{-4}	m
Substrate density	1.71×10^3	kg/m^3
Catalytic surface area per unit monolith volume	18,930	m^2/m^3
Substrate heat capacity	$1071 + 0.156 \cdot T_s - 3.435 \times 10^7 / T_s^2$	J/kgK
Substrate thermal conductivity	1.675	W/mK
Gas heat capacity	$1009.1248 + 0.2182 \cdot T_g$	J/kgK
Gas thermal conductivity	$2.269 \times 10^{-4} \cdot T_g^{0.832}$	W/mK

The transient energy conservation equation in the solid phase accounts for the convective heat transfer with the exhaust gas, axial heat conduction, and reaction exothermy. The corresponding equation is described as:

$$(1-\varepsilon) \cdot \rho_s \cdot c_{p,s} \cdot \frac{\partial T_s}{\partial t} =$$
$$(1-\varepsilon) \cdot \lambda_s \cdot \frac{\partial^2 T_s}{\partial x^2} - h_t(x) \cdot GSA \cdot (T_s - T_g) + a(x) \cdot \sum_{k=1}^{N_R} (-\Delta H_k) \cdot r_k \quad (4)$$

The reaction rate on the surface for each species is linked to the local species mass transfer to/from the exhaust gas by the following equation

$$(1-\varepsilon) \cdot \rho_g \cdot \frac{\partial w_{i,s}}{\partial t} =$$
$$\rho_g \cdot k_{m,i}(x) \cdot GSA \cdot (w_{i,g} - w_{i,s}) - a(x) \cdot M_i \cdot \sum_{k=1}^{N_R} v_{ik} \cdot r_k \quad (5)$$

The Danckwerts boundary conditions at the inlet and outlet for a dual monolithic catalytic converter with the space between monoliths, i.e., with the air-gap of 0.0162 m, for solving the aforementioned governing equations are:

$$\varepsilon \cdot \lambda_g \cdot \frac{\partial T_g}{\partial x}\bigg|_{x=0} = \frac{m}{A} \cdot c_{p,g} \cdot (T_g - T_g^{in}) \qquad \frac{\partial T_g}{\partial x}\bigg|_{x=L} = 0 \quad (6)$$

$$\varepsilon \cdot D_i \cdot \rho_g \cdot \frac{\partial w_{i,g}}{\partial x}\bigg|_{x=0} = \frac{m}{A} \cdot (w_{i,g} - w_{i,g}^{in}) \qquad \frac{\partial w_{i,g}}{\partial x}\bigg|_{x=L} = 0 \quad (7)$$

$$\frac{\partial T_s}{\partial x}\bigg|_{x=0} = 0 \qquad \frac{\partial T_s}{\partial x}\bigg|_{x=L} = 0 \quad (8)$$

The governing equations (1), (2), and (4) are discretized with the finite volume method and solved in conjunction with the Danckwerts boundary conditions given by equations (6)-(8) for dual monolithic catalytic converters. Equations (1), (2), and (4) are discretized by using a dense uniform grid and employing the control volume approach and the backward difference scheme in time and the central implicit difference scheme in the spatial direction. The equations are solved by using a standard tri-diagonal matrix algorithm (TDMA) with a successive line under-relaxation scheme. Broyden's method [11], which is a quasi-Newtonian method for numerical solution of nonlinear equations, is used to solve the nonlinear systems of equation (5) for the chemical species concentrations on the monolith surface. The input data for the catalyst model are listed in Table 1.

Table 2 Reaction scheme and rate expressions.

	Reaction	Rate expression
1	$CO + 0.5O_2 \rightarrow CO_2$	$r_1 = k_{0,1} e^{-E_{a,1}/R_g T_s} c_{CO} c_{O_2} / G_1$
2	$C_3H_6 + 4.5O_2 \rightarrow 3CO_2 + 3H_2O$	$r_2 = k_{0,2} e^{-E_{a,2}/R_g T_s} c_{C_3H_6} c_{O_2} / G_1$
3	$CH_4 + 2O_2 \rightarrow CO_2 + 2H_2O$	$r_3 = k_{0,3} e^{-E_{a,3}/R_g T_s} c_{CH_4} c_{O_2} / G_1$
4	$H_2 + 0.5O_2 \rightarrow H_2O$	$r_4 = k_{0,4} e^{-E_{a,4}/R_g T_s} c_{H_2} c_{O_2} / G_1$
5	$CO + H_2O \rightarrow CO_2 + H_2$	$r_5 = k_{0,5} e^{-E_{a,5}/R_g T_s} c_{CO} c_{H_2O} Eq_5 / G_1$
6	$C_3H_6 + 3H_2O \rightarrow 3CO + 6H_2$	$r_6 = k_{0,6} e^{-E_{a,6}/R_g T_s} c_{C_3H_6} c_{H_2O} Eq_6 / G_1$
7	$CH_4 + H_2O \rightarrow CO + 3H_2$	$r_7 = k_{0,7} e^{-E_{a,7}/R_g T_s} c_{CH_4} c_{H_2O} Eq_7 / G_1$
8	$CO + NO \rightarrow CO_2 + 0.5N_2$	$r_8 = k_{0,8} e^{-E_{a,8}/R_g T_s} c_{CO}^m c_{NO}^{0.5} / G_2$
9	$C_3H_6 + 9NO \rightarrow 3H_2O + 3CO_2 + 4.5N_2$	$r_9 = k_{0,9} e^{-E_{a,9}/R_g T_s} c_{C_3H_6} c_{NO} / G_1$
10	$H_2 + NO \rightarrow H_2O + 0.5N_2$	$r_{10} = k_{0,10} e^{-E_{a,10}/R_g T_s} c_{H_2} c_{NO} / G_1$

Inhibition term

$$G_1 = T_s (1 + K_1 c_{CO} + K_2 c_{HC})^2 (1 + K_3 c_{CO}^2 c_{HC}^2)(1 + K_4 c_{NO}^{0.7}),$$

$$G_2 = T_s^{-0.17} (T_s + K_5 c_{CO})^2, \quad K_j = k_{a,j} \exp(-\Delta H_{a,j} / R_g T_s)$$

Auxiliary quantities

$$Eq_5 = 1 - \frac{c_{CO_2} c_{H_2}}{c_{CO} c_{H_2O} K_p(T)}, \quad Eq_6 = 1 - \frac{c_{CO}^3 c_{H_2}^6}{c_{C_3H_6} c_{H_2O}^3 K_p(T)}, \quad Eq_7 = 1 - \frac{c_{CO} c_{H_2}^3}{c_{CH_4} c_{H_2O} K_p(T)}$$

$$m = -0.19[1 - 6.26 e^{-m_1 c_{CO}}] \text{ where } m_1 \text{ is a tunable factor } (m_1 = 3,500)$$

Chemical Reaction Kinetics Model

The main oxidation reactions occurring in three-way catalysts involve carbon monoxide (CO) and unburned hydrocarbons (HC). Methane (14%) and Propylene (86%) are used to model "slow" and "fast" oxidizing hydrocarbons, respectively. Hydrogen (H_2) oxidation is taken into account, due to the substantial heat production associated with it, while its reaction kinetics are simple to treat, since they are closely related to CO oxidation kinetics. Here, H_2 concentration is assumed to be 36% of CO concentration. In the present model, the oxidation reaction rates of CO, H_2, and HC are based on the expressions by Voltz *et al.* [12].

Water-gas shift reaction and the steam reforming reactions are incorporated into the reaction scheme [13]. To account for the chemical equilibrium of the steam reforming and water-gas shift reactions, an additional factors (Eq_5, Eq_6, and Eq_7) are considered in the respective reaction rate expressions. Obviously, negative values for the additional factors imply that the water-gas shift and steam reforming reactions are thermodynamically not possible and the reaction rates are zero.

The simultaneous reduction of NO is considered by three different reaction pathways. Among those reactions, the one involving CO is considered to be the main path. The NO reduction by CO is modeled using an empirical reaction rate expression [14], which predicts a variable order of reaction for the CO oxidation from NO, depending on CO concentration. The chemical reaction scheme and kinetics rate expressions of the three-way catalyst used in this study are listed in Table 2.

Optimization Procedure and Problem Formulation

A flow chart of the optimal design process is depicted in Figure 2. The optimal design variables of the catalytic converter are obtained through three modules: analysis, optimization, and control. The analysis module is used to calculate the objective functions with a one-dimensional single channel model and the Romberg integration method [15]. This module obtains new design variables from the control module, produces the CO cumulative emissions and the integral value of a catalyst distribution function a(x) over the monolith volume, and provides objective function values to the control module. The optimal design variables for minimizing the objective functions are determined by the optimization module with μGA. The control module manages the optimal design process that takes place mainly in the analysis and optimization modules. The optimization procedures are discussed in more detail by Kim and Kim [8]. The mathematical formulation of the nonlinear optimization problem is as follows:

$$find \quad X = \{\alpha, \beta\}^T \tag{9}$$

$$to\ minimize \quad \sum_{k=1}^{N} F_k(X) \tag{10}$$

$$subject\ to \quad -10 \le \alpha, \beta \le 10 \tag{11}$$

As mentioned above, two objective functions are considered in this study and described as follows:

$$CCE = \int_0^t CE\ dt \tag{12}$$

$$CSA = \left\{ \left[a_o - \frac{1}{V_m} \int^{V_m} a(x)\ dV_m \right]^2 \right\}^{1/2} \tag{13}$$

with

$$a(x) = \exp(\alpha - \beta \cdot x) \tag{14}$$

where CE, CCE, and CSA are the CO emissions per unit time, objective functions $F_1(X)$ and $F_2(X)$. $F_1(X)$ represents the CO cumulative emissions during FTP-75 test cycle. $F_2(X)$ indicates the difference between the integral value of a catalyst distribution function a(x) over the monolith volume and catalytic surface area per unit monolith volume a_o. For the baseline catalytic converter with the uniform axial catalyst distribution, the coefficients α and β included in the catalyst distribution function a(x) are 5.243 and 0, respectively.
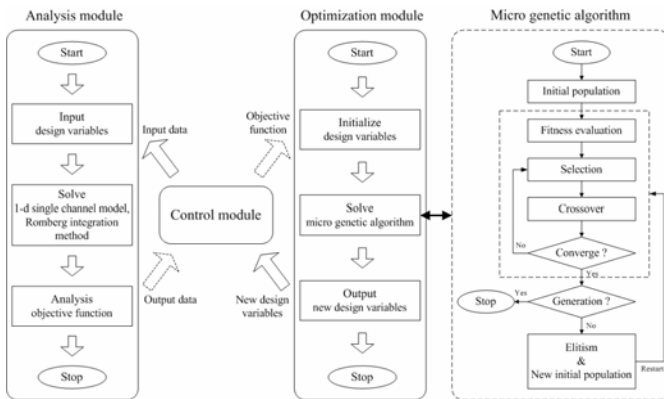

Figure 2 Flow chart of the optimal design process and micro genetic algorithm.

RESULTS AND DISCUSSION

Model Validation

A series of experiments on a 1.5 L four cylinder engine are performed to validate the reaction mechanism on real engine exhaust gas over the first 200 s of the FTP-75 cycle. As shown in Table 2, the kinetic parameters, activation energy $E_{a,k}$, and the pre-exponential factor $k_{0,k}$, of the global reaction mechanism are tuned to find a compromise in agreement between computed and measured data. The under-floor catalyst system is tandem comprised of 0.895 L front and rear catalysts with the space between monoliths of 0.0162 m, as listed in Table 1. A 5:1 Pt/Rh catalyst at 26.9 g/ft^3 loading is supported on each substrate with cell geometry of 400 cpsi and 6.5 mil wall.

Figure 3 presents the computed and measured gas and wall temperatures at the inlet and exit of the front and rear monoliths during the first 200 s of FTP-75. Apparently, the mathematical model shows a remarkable ability in matching the behavior of the converter. As shown in Figure 3(a), just after the deceleration (about 115 sec) the outlet gas temperature of front monolith becomes substantially higher than inlet gas temperature because of exothermic reaction and axial heat conduction through the wall. With respect to wall temperature at the inlet of monoliths depicted in Figure 3(b), the inlet wall temperature of rear monolith achieved higher temperature than the front monolith due to the faster convective heat transfer of chemical exotherms in the front monolith towards downstream.
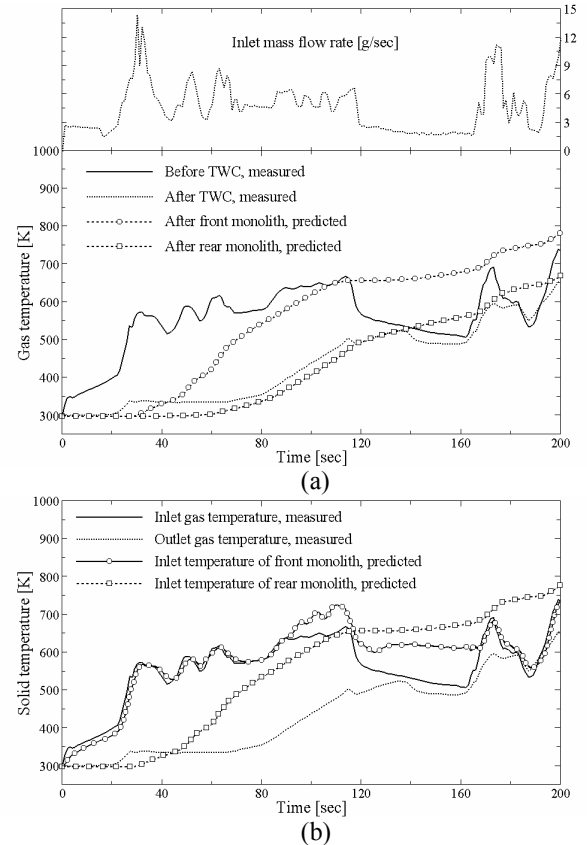

(a)

(b)

Figure 3 Transient profiles of mass flow rate, gas and wall temperatures during the first 200 s of FTP-75 drive cycle: (a) mass flow rate and gas temperature; (b) wall temperature.
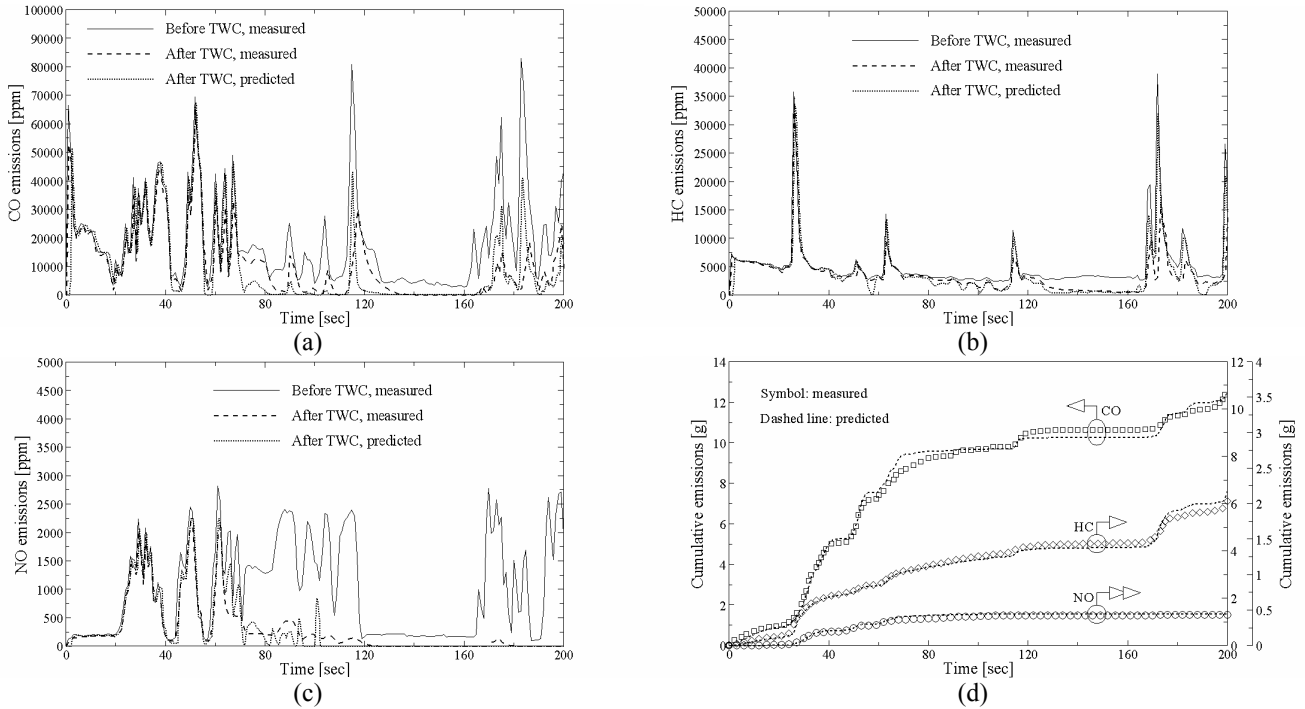
Figure 4 Computed and measured species emissions and cumulative species emissions at the exit of the converter during the first 200 s of FTP-75 cycle: (a) CO emissions; (b) HC emissions; (c) NO emissions; (d) cumulative species emissions.

The computed instantaneous CO, HC, and NO emissions are plotted in Figure 4(a), (b), and (c), respectively, and compared to experimental data. And the cumulated pollutant mass of CO, HC, and NO is compared to measured data during the first 200 s of FTP-75 in Figure 4(d), showing good agreement for all species. According to the experimental results, catalyst-out emissions over the FTP-75 drive cycle were 12.49, 6.11, and 0.44 g for CO, HC, and NO emissions, respectively. In comparison, the computed cumulative emissions for CO, HC, and NO are 12.53, 6.57, and 0.45 g, respectively.

Optimal Axial Distribution of Catalyst

The optimal design for the optimal axial distribution of the catalyst is performed by solving the multi-objective optimization problems which are aimed at minimizing the CCE and CSA. The optimal catalyst distributions, cumulative CO emissions for the optimal profiles of axial catalyst distribution, and wall temperature at the inlet of monoliths are demonstrated in Figure 5. Here the optimal coefficients α and β are 7.986 and 1.72 for optimal A, 9.013 and 4.8 for optimal B, and 9.443 and 7.38 for optimal C, respectively.

As illustrated in Figure 5(a), the catalyst surface area of the optimal distributions is significantly higher in the upstream section of the monolith. The catalyst surface area in the downstream section is lower than that of the uniform distribution. It can be seen that the concentration degree of the catalyst surface area in the upstream section for optimal A is lowest in the three optimal profiles. The cumulative CO, HC, and NO emissions during the first 140 s of the FTP-75 test cycle for three optimal catalyst distributions are reduced by approximately 21%, 12%, and 49%, respectively, compared to those of the uniform catalyst distribution shown in Figure 5(b). Figure 5(c) represents the

CO cumulative emissions and the concentrated amount of the catalyst in the upstream section for several axial catalyst distributions. For all catalyst distributions shown in Figure 5(c), the integral value of a catalyst distribution function a(x) over the monolith volume is almost the same as the value of a_0 with a maximum difference of 0.03%, i.e., $|CSA/a_0|_{max} \times 100\%$. As α increases from 5.243 (uniform catalyst distribution) to 7.986 (optimal A), the cumulative CO emissions are greatly reduced, while the dimensionless catalyst surface area in the upstream section of the converter (that is, $a(0)/a_0$) increases gradually. However, $a(0)/a_0$ increases dramatically with increasing α above 5.243 (saturation point), while the variations in the cumulative CO emissions are negligibly small due to the mass transport limitations. Also, the temporal evolution of inlet wall temperature in the front and rear monoliths for the optimal axial catalyst distribution is illustrated in Figure 5(d), and compared to that of uniform distribution. It can be seen that the light-off performance of the converter with optimal profile is significantly better than that of uniform distribution.

CONCLUSION

In this study, the optimal design of a longitudinal noble metal distribution for a fixed amount of catalyst was investigated to obtain the best performance of a dual monolithic catalytic converter by using a micro genetic algorithm. With a one-dimensional transient catalyst model, the optimal design analysis was performed by solving the transient thermal and conversion characteristics of a dual monolithic catalytic converter with Pt/Rh catalysts during FTP-75 cycle.

The catalyst surface area of the optimal distribution is greatly higher in the upstream section of the monolith, while in
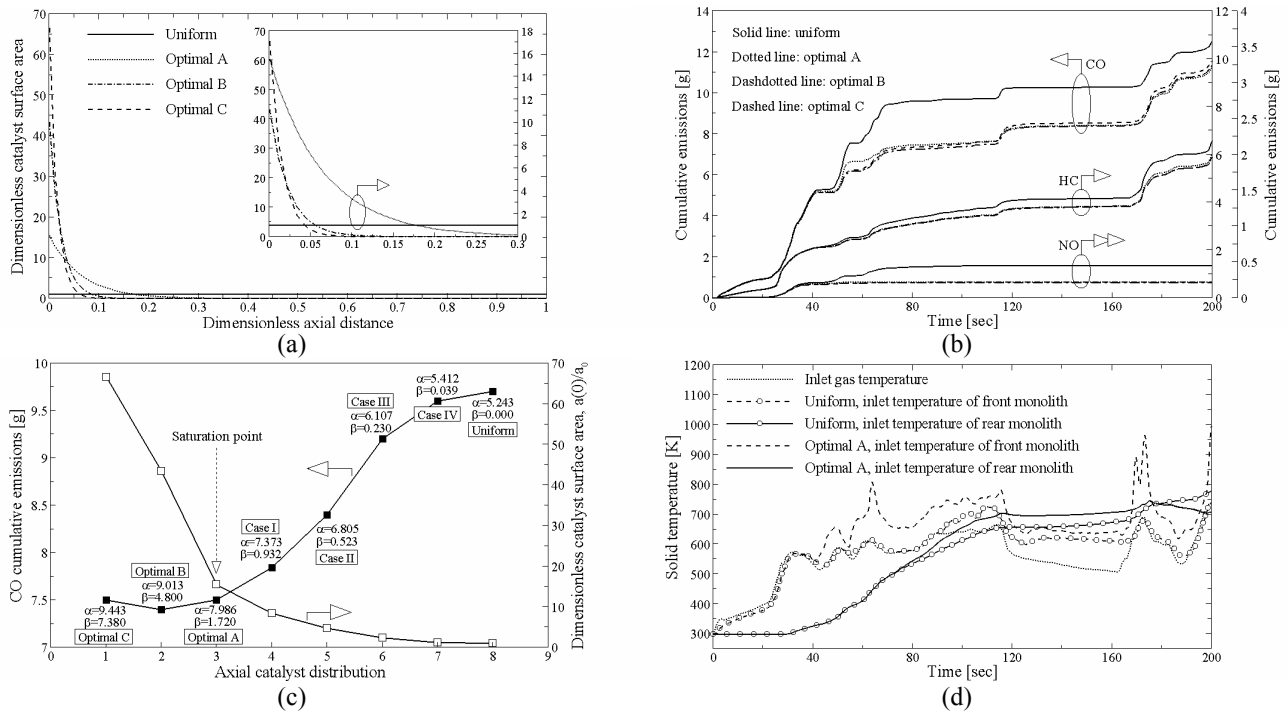
Figure 5 Optimal profiles of axial catalyst distribution, and cumulative species emissions and solid temperature during the first 200 s of FTP-75 cycle: (a) optimal catalyst distributions; (b) cumulated pollutant mass; (c) CO cumulative emissions and concentration degree of the catalyst in the upstream section with respect to axial catalyst distribution; (d) wall temperature at the inlet of monoliths.

the downstream section it is lower than that of the uniform distribution. However, it is noted that in the upstream section of the converter the catalyst surface area greater than saturation point (optimal A) has little effect on the cumulative CO emissions due to the mass transport limitations. The optimal coefficients α and β included in the catalyst distribution function $a(x)$ are 7.986 and 1.72, respectively. Here, the cumulative CO, HC, and NO emissions during the first 140 s of the FTP-75 cycle are reduced by approximately 21%, 12%, and 49%, respectively, as compared to those obtained with the uniform catalyst distribution.

ACKNOWLEDGMENT

REFERENCES

[1] Oh, S.H., and Cavendish, J.C., Transients of monolithic catalytic converters: response to step changes in feedstream temperature as related to controlling automobile emissions, *Industrial and Engineering Chemistry Process Design and Development*, Vol. 21, 1982, pp. 29-37

[2] Gavriilidis, A., Varma, A., and Morbidelli, M., Optimal distribution of catalyst in pellets, *Catalysis Reviews-Science and Engineering*, Vol. 35, 1999, pp. 399-456

[3] Psyllos, A., and Philippopoulos, C., Performance of a monolithic catalytic converter used in automotive emission control: the effect of longitudinal parabolic active metal distribution, *Industrial and Engineering Chemistry Research*, Vol. 32, 1993, pp. 1555-1559

[4] Cominos, V., Gavriilidis, A., Theoretical investigation of axially non-uniform catalytic monoliths for methane combustion, *Chemical Engineering Science*, Vol. 56, 2001, pp.3455-3468

[5] Melis, S., Varma, A., and Pereira, C.J., Optimal distribution of catalyst for a case involving heterogeneous and homogeneous reactions, *Chemical Engineering Science*, Vol. 52, 1997, pp. 165-169

[6] Khanaev, V.M., Borisova, E.S., Noskov, A.S., Optimization of the active component distribution through the catalyst bed for the case of adiabatic reactor, Chemical Engineering Science, Vol. 60, 2005, pp. 5803-5808

[7] Tronci, S., Baratti, R., and Gavriilidis, A., Catalytic converter design for minimisation of cold-start emissions, *Chemical Engineering Communications*, Vol. 173, 1999, pp. 53-77

[8] Kim, Y.-D., and Kim, W.-S., Optimum design of an automotive catalytic converter for minimization of cold-start emissions using a micro genetic algorithm, *International Journal of Automotive Technology*, Vol. 8, 2007, pp. 563-573

[9] Fuller, E.N., Ensley, K., and Giddings, J.C., Diffusion of halogenated hydrocarbons in helium: the effect of structure on collision cross sections, *Journal of Physical Chemistry*, Vol. 73, 1969, pp. 3679-3685

[10] Kirchner, T., and Eigenberger, G., On the dynamic behavior of automotive catalysts, *Catalysis Today*, Vol. 38, 1997, pp. 3-12

[11] Broyden, C.G., A class of methods for solving nonlinear simultaneous equations, *Mathematics of Computation*, Vol. 19, 1965, pp. 577-593

[12] Voltz, S.E., Morgan, C.R., Liederman, D., and Jacob, S.M., Kinetic study of carbon monoxide and propylene oxidation on platinum catalysts, *Industrial and engineering chemistry product research and development*, Vol. 12, 1973, pp. 294-301

[13] Tsinoglou, D.N., and Koltsakis, G.C., Effect of perturbations in the exhaust gas composition on three-way catalyst light off, *Chemical Engineering Science*, Vol. 58, 2003, pp. 179-192

[14] Oh, S.H., Effects of Cerium Addition on the CO-NO reaction kinetics over alumina-supported rhodium catalysts, *Journal of Catalysis*, Vol. 124, 1990, pp. 477-487

[15] Zarowski, C.J., An introduction to numerical analysis for electrical and computer engineers, John Wiley & Sons, New York, 2004